Biochimica et Biophysica Acta 1828 (2013) 1973–1981

Contents lists available at SciVerse ScienceDirect

Biochimica et Biophysica Acta

journal homepage: www.elsevier.com/locate/bbamem

Cation selectivity of the plasma membrane of tobacco protoplasts in the electroporated state

Lars H. Wegner *

Karlsruhe Institute of Technology, Institute for Pulsed Power and Microwave Technology (IHM), Campus North, 76344 Eggenstein-Leopoldshafen, Germany
Botanical Institute I—Molecular Cell Biology, Campus South, 76131 Karlsruhe, Germany

ARTICLE INFO

Article history:
Received 4 January 2013
Received in revised form 8 April 2013
Accepted 9 April 2013
Available online 17 April 2013

Keywords:
BY-2 (bright yellow-2)
Cation selectivity
Electroporation
Ionic diameter
Pore diameter

ABSTRACT

Cation selectivity of the cellular membrane of tobacco culture cells (cell line 'bright yellow-2') exposed to pulsed electric fields in the millisecond range was investigated. The whole cell configuration of the patch clamp technique was established on protoplasts prepared from these cells. Ion selectivity of the electroporated membrane was investigated by measuring the reversal potential of currents passing through field-induced pores. To this end the membrane was hyper- or depolarized for 10 ms (prepulse); subsequently the voltage was driven to opposite polarity at a constant rate (+40 or −40 mV/ms, respectively). The experiment was started by polarizing the membrane to moderately negative or positive voltages (prepulse potential ±150 mV) that would not induce pore formation. Subsequently, an extended voltage range was scanned in the porated state of the membrane (prepulse potential ±600 mV). IV curves in the porated and the non-porated state (obtained at the same prepulse polarity) were superimposed to determine the voltage at which both curves intersected ('Intersection potential'). Using a modified version of the Goldmann–Hodgkin–Katz equation relative permeabilities to Ca^{2+} and various monovalent alkali and organic cations were calculated. Pores were found to be fairly cation selective, with a selectivity sequence determined to be $Ca^{2+} > Li^{+} > Rb^{+} \approx K^{+} \approx Na^{+} > TEA^{+} \approx TBA^{+} > Cl^{-}$. Relative permeability to monovalent cations was inversely related to the ionic diameter. By fitting a formalism suggested by Dwyer at al. (J. Gen. Physiol. 75 (1980), 469–492) the effective average diameter of field induced pores was estimated to be about 1.8 nm. Implications of these results for biotechnology and electroporation theory are discussed.

1. Introduction

Permeabilization of the cellular membrane by brief (ns to ms) exposure to an electrical field is a frequently used method in biotechnology, e.g. for the introduction of macromolecules like DNA into cells. More recently, medical application (e.g. in gene therapy and cancer treatment) has received increasing attention. But despite about 40 years of research since this technique was initially introduced [1,2], our understanding of how electrical fields interact with the membrane on the molecular scale, and our knowledge of membrane properties in the 'electropermeabilized' (or 'electroporated') state, is still far from being comprehensive. Molecular simulation studies of the membrane in the presence of a strong electric field (at least about 5 kV/cm, depending on the pulse length) rendered support for models that involve the formation of short-lived, lipid-lined (nano) pores in the membrane [3,4]. This is implied by the term 'electroporation' that is favoured by most researchers working in the field. Most of the available experimental data are also in accordance with this model. I will adopt the terminology here for convenience, even though it has to be kept in mind that experimental data generally considered as a definitive proof of this concept have not been provided yet.

Among other things, we lack detailed information on the (ion) selectivity of the membrane in the electroporated state. Selectivity data are important for applied research since they provide evidence which substances are likely to permeate into the cell most easily (and which are less likely to do so) when a cell is exposed to pulsed electric fields (PEFs). From a basic research viewpoint, selectivity data help us to understand the properties of transport pathways through the membrane. Detailed studies on this subject were undertaken by Pakhomov and coworkers using the whole cell patch clamp technique [5–7]. However, these studies focused on the properties of the membrane *after* the application of nanosecond PEFs. Using the same technique, Wegner et al. [8,9] and Wegner and Schönwälder [10] investigated membrane poration *during* the application of ms-pulses on protoplasts

Abbreviations: a, ion activity; BTP, Bis-Tris propane; BY-2, bright yellow-2; c_{cell}, cell capacitance; EGTA, ethylene glycol tetraacetic acid; E_I, intersection potential; E_x, Nernst potential of the ion x; LJP, liquid junction potential; PEF, pulsed electric field; NtORK, Nicotiana tabacum outward rectifying K^+ channel; IV curve, current–voltage curve; SEM, standard error of the mean; TEA, tetraethylammonium; TBA, tetrabutylammonium; δ_{pore}, effective pore diameter; δ_x, ionic diameter of ion x

* Plant Bioelectrics Group, Karlsruhe Institute of Technology, Campus North, Building 630, Hermann-v-Helmholtz Platz 1, 76344 Eggenstein-Leopoldshafen, Germany. Tel.: +49 721 24302; fax: +49 721 22823.
E-mail address: lars.wegner@ihm.fzk.de.

0005-2736/$ – see front matter © 2013 Elsevier B.V. All rights reserved.
http://dx.doi.org/10.1016/j.bbamem.2013.04.010

isolated from tobacco culture cells (cell line Bright Yellow-2). It was found that polarization beyond threshold values of about −250 mV and +200 mV, respectively, led to an at least 50 fold increase in membrane conductance with respect to the value obtained in the physiological voltage range. By superimposing current voltage relations obtained by voltage ramp protocols in the physiological and the porated state, the intersection potential (the crossing point of the IV curves) could be inferred as identifying the voltage at which currents passing through pores reversed polarity (for a detailed discussion on the validity of this approach, see 4.1). These measurements provided evidence that the electroporated membrane is surprisingly cation selective and conducts anions poorly [8,9].

Here, I complete the dataset on ion selectivity of BY-2 protoplasts in the electroporated state by testing monovalent cations of varying size and mobility. Moreover, membrane permeability to Ca^{2+} is separately tested. From these data relative ion permeabilities can be calculated using an extended version of the Goldman-Hodgkin-Katz equation [11], and based on these data a selectivity sequence was established. These data have practical relevance for optimizing the medium composition when electroporation is applied in biotechnology and medicine, and provides us with some important hints concerning the molecular mechanisms of transport across the membrane. These aspects are addressed in the Discussion.

2. Materials and methods

2.1. Cultivation of tobacco culture cells, preparation of protoplasts and electrophysiology

Patch-clamp experiments in the whole cell configuration were performed on protoplasts prepared from calli of the tobacco cell line Bright Yellow-2 (BY-2). Cell culture and protoplast preparation were performed as described in detail in previous publications [8,9]. The standard patch clamp setup used here was identical to the one used in these preceding studies. Micropipettes were fabricated from borosilicate glass (No. 34500 99; Kimble, Rockwood, TN, USA) with a two-step-procedure using a Narishige puller (PE-21, Narishige, Tokyo, Japan). Voltage was controlled and current recorded with an EPC-10 amplifier (HEKA electronic, Lambrecht, Germany). In order to calculate the actual trans-membrane voltage drop from the applied command voltage at supra-physiological voltages it was important to take into account the voltage drop at the access resistance, i.e. the junction between pipette and cell interior, (the so-called 'voltage divider effect'; [8]). The applied command voltage (V_{comm}) had to be corrected for this value to assess the actual trans-membrane voltage drop (V_M) when a voltage pulse (ΔV_{comm}) was applied (for more details, see [8])

$$V_M(t) = V_{comm}(t) - [I(t)/I_0] * \Delta V_{comm} \quad (1)$$

I(t) is the current as a function of time. The current amplitude of the capacitive current relaxation, I_0, was obtained from the time course of the capacitive current relaxation I_{cap} (t) upon a stepwise increase or decrease of voltage by fitting the following equation to the data:

$$I_{cap}(t) = I_0 * \exp(-t/\tau) \quad (2)$$

The mathematical routine used for this correction can be obtained from the previous publication [8].

The current response of a cell to a voltage ramp protocol (continuous change of voltage with time) consists of a capacitive component (I_{cap}) and a resistive component (I_{res} (t)). Only the latter is relevant for the determination of the intersection potential. Hence, the capacitive component has to be subtracted from the overall current I_{ramp} (t) according to:

$$I_{res}(t) = I_{ramp}(t) - I_{cap} = I_{ramp}(t) - c_{cell} * dV_M/dt \quad (3)$$

c_{cell} is the cell capacitance (for more details see [8]).

2.2. Patch clamp solutions, calculation of ion activities, correction for liquid junction potentials

The patch clamp solutions used in this study were designed to determine relative permeabilities for a range of monovalent cations at maximum resolution. To this end, a steep concentration gradient between pipette and bath solution was imposed (250 mM *versus* 12.5 mM monovalent cation concentration). In another combination of solutions, monovalent cations were completely replaced by Ca^{2+}. The composition of the various solutions used in this study is summarized in Table 1. Free Ca^{2+} concentrations in the pipette solutions were calculated using the program 'calcium' written by Führ et al. [12]. Activities were calculated from ion concentrations according to the formalism of Davies [13]. Liquid junction potentials for the various combinations of solutions used here (Table 2) were determined experimentally using the protocol of Neher [14] and were corrected for by using the corresponding function in the data acquisition program Patchmaster (HEKA electronics), or *ex post* during data evaluation.

2.3. Calculation of relative permeabilities

Relative permeabilities for the major ions of the patch clamp solutions are accessible from intersection potentials (i.e. reversal potentials of the current voltage relations associated with field induced pores) by the Goldman-Hodgkin-Katz equation. The original version of this equation only takes monovalent ions into account. However, for this study the Ca^{2+} permeability of the pores was of major importance. Therefore, an extended version of the equation developed by Piek [11] that includes Ca^{2+} permeability was used here:

$$E_I = \frac{RT}{F} \ln\left(\frac{-b + \left(b^2 - 4ac\right)^{0.5}}{2a}\right) \quad (4)$$

With

$$a = 4P_{Ca2+}\left[Ca^{2+}\right]_{in} + P_{x+}\left[X^+\right]_{in} + P_{Cl-}[Cl^-]_{ex}$$

$$b = P_{x+}\left[X^+\right]_{in} - P_{x+}\left[X^+\right]_{ex} + P_{Cl-}[Cl^-]_{ex} - P_{Cl-}[Cl^-]_{in}$$

$$c = -\left(P_{x+}\left[X^+\right]_{ex} + 4P_{Ca2+}\left[Ca^{2+}\right]_{ex} + P_{Cl-}[Cl^-]_{in}\right)$$

P_x, P_{Cl-} and P_{Ca2+} are the membrane permeabilities for the respective monovalent cation(s) X^+, chloride and Ca^{2+}, respectively. R, T and F have their usual meaning.

The equation was solved numerically using an open access program designed by A. Brünner (http://www.arndt-bruenner.de/mathe/scripts/gleichungssysteme2.htm).

3. Results

3.1. Steady-state current–voltage relations of BY-2 protoplasts

Electrophysiological properties of BY-2 protoplasts have been characterized in detail previously, and their spectrum of ion channels is well documented in the literature [8,15–17]. However, methods of cell culture and protoplast preparation, as well as the composition of pipette and bath solutions that were optimized here for studying

Table 1
Composition of patch clamp solutions used in this study, and calculated activities of the major ions[a].

Medium	Monovalent cation (X)	[XCl] (mM)	[$CaCl_2$] (mM)	[$MgCl_2$] (mM)	[EGTA] (mM)	[BTP] (mM)	[MES] (mM)	a_{x+} (mM)	a_{Cl-} (mM)	a_{Ca2+} (mM)
P1	K^+	250	3.91 (free Ca^{2+}: 0.1 μM)	2.55 (free Mg^{2+}: 2 mM)	10	2		127	131	
P2	TEA^+									
P3	TBA^+									
P4	Rb^+									
P5	Na^+									
P6	Li^+									
P7	-	-	253	2.55	10	2		-	339	48
B1	K^+	12.5	5	2	-	-	2	10	21	2.3
B2	TEA^+									
B3	TBA^+									
B4	-	-	17.5	2	-	-	2	-	32	8

[a] Osmolalities of solutions determined with a vapour pressure osmometer ranged from 480 to 600 mosmol kg^{-1}. Osmolality of the bath solution was adjusted to a value that was slightly lower than that of the pipette medium by adding appropriate amounts of mannitol. PH in P and B media was adjusted to 7.2 and 5.8, respectively, by adding BTP or MES. For calculation of ion activities, see text. a = ion activity.

cation selectivity of the membrane, differed somewhat from those used in previous studies. Steep concentration gradients of monovalent cations (250 mM *versus* 12.5 mM in pipette and bath, respectively) were imposed to improve the resolution of the selectivity measurements. Therefore, it seemed appropriate to start this study by measuring steady state current voltage relations in the physiological voltage range. To this end, the clamped voltage was stepped in 20 mV increments to various potentials ranging from −100 to +120 mV (well below the threshold for field induced pore formation; [8]) for 1.5 s. Fig. 1A and B show the voltage protocol and the current response, respectively, of a protoplast when K^+ was included as the monovalent cation in both pipette and bath solution. Note that the IV curve was strongly outward rectifying with K^+ in the pipette medium (Fig. 1E, solid squares); large outward currents carried by the Shaker-type outward-rectifying channel NtORK [15] were activated, whereas inward currents remained small. In fact, in the majority of the protoplasts tested here NtORK dominated the membrane conductance in the physiological voltage range. Note that currents activated with a delay; the activation kinetics was slightly sigmoidal, as expected for a tetrameric channel protein with four independent gates [18]. No outward rectification was observed when K^+ in both pipette and bath solution was replaced by large organic cations TEA^+ and TBA^+ (Fig. 1C and D, respectively). Obviously, the permeability of the membrane to these cations is poor in the voltage range considered here (see also IV curves in Fig. 1E), and these ions did not pass through the outward rectifying K^+ channels.

Table 2
Intersection potentials determined for the various combinations of solutions used in this study, and negative values of liquid junction potentials[1].

Combinations of media	E_I (mV)		(−)Liquid junction potential (mV)
	Negative-going prepulse, ramp +40 mV/ms (c.v.)	Positive-going prepulse, ramp -40 mV/ms (c.v.)	
P1/B1	-24 ± 3^a (n = 18)	-20 ± 6^a (n = 3)	<2
P2/B2	-10 ± 3^b (n = 17)	-6 ± 5^b (n = 5)	13
P3/B3	-13 ± 4^b (n = 13)	-11 ± 4^b (n = 3)	20
P4/B1	-27 ± 8^a (n = 6)	n.d.	<2
P5/B1	-24 ± 5^a (n = 6)	n.d.	4
P6/B1	-39 ± 7^c (n = 9)	n.d.	5
P7/B4	-6 ± 3^b (n = 7)	-6 ± 4^b (n = 5)	9

[1] c.v. = command voltage; mean E_I values ± SE are given; superscripts a, b, and c indicate significant difference according to Student's t-test at the 0.05 level.

Subsequently, these experiments were repeated after substituting K^+ in the pipette solution with either Na^+ or Rb^+, whereas K^+ in the bath remained unchanged (so-called bi-ionic conditions). Outward currents with kinetics characteristic for NtORK were elicited in the presence of alkali cations other than K^+, indicating that the channel was permeable to these cations. However, the current densities obtained with Na^+ and Rb^+ were significantly lower than those in the presence of K^+ (Fig. 1F).

3.2. Current–voltage relation elicited by 10-ms-voltage pulses

By contrast, when current voltage relations were measured on a wider voltage range for a pulse length of 10 ms, measurements with K^+ and the organic cation TEA^+ rendered IV curves with very similar shape (Fig. 2). Results of this kind were also obtained with TBA^+ (not shown). Polarization of the membrane beyond threshold values induced a large increase in conductance both in the positive and negative direction, as described previously [8], apparently due to the formation of field-induced pores. The data indicated that these pores also permeated organic cations, in sharp contrast to NtORK. This finding provides another piece of evidence that these K^+ channel proteins do not provide the molecular basis of the field-induced increase of membrane conductance (compare [8]).

3.3. Selectivity of field-induced pores to monovalent cations

The focus of this study is on the cation selectivity of the plasma membrane at extreme (supra-physiological) voltages. Selectivity was tested by applying a 10-ms-prepulse to −600 or +600 mV command voltage and subsequently forcing currents through field-induced pores while continuously changing the command voltage at a constant rate. Note that pores started to close within a few milliseconds once the membrane potential entered the intermediate voltage range. Therefore, 'fast' ramps (slope ±40 mV) had to be imposed to make sure that a sufficiently large fraction of pores prevailed while the membrane potential passed through the physiological voltage range. Background currents (including those due to an imperfect seal and ion transporters in the membrane, compare Fig. 1) were taken into account by a preceding ramp experiment that started with a prepulse to ±150 mV (that would not induce pore formation, compare Fig. 2). Current voltage relations obtained from such a pair of ramp experiments were superimposed (Fig. 3). The voltage at which the IV curves intersected (the 'intersection

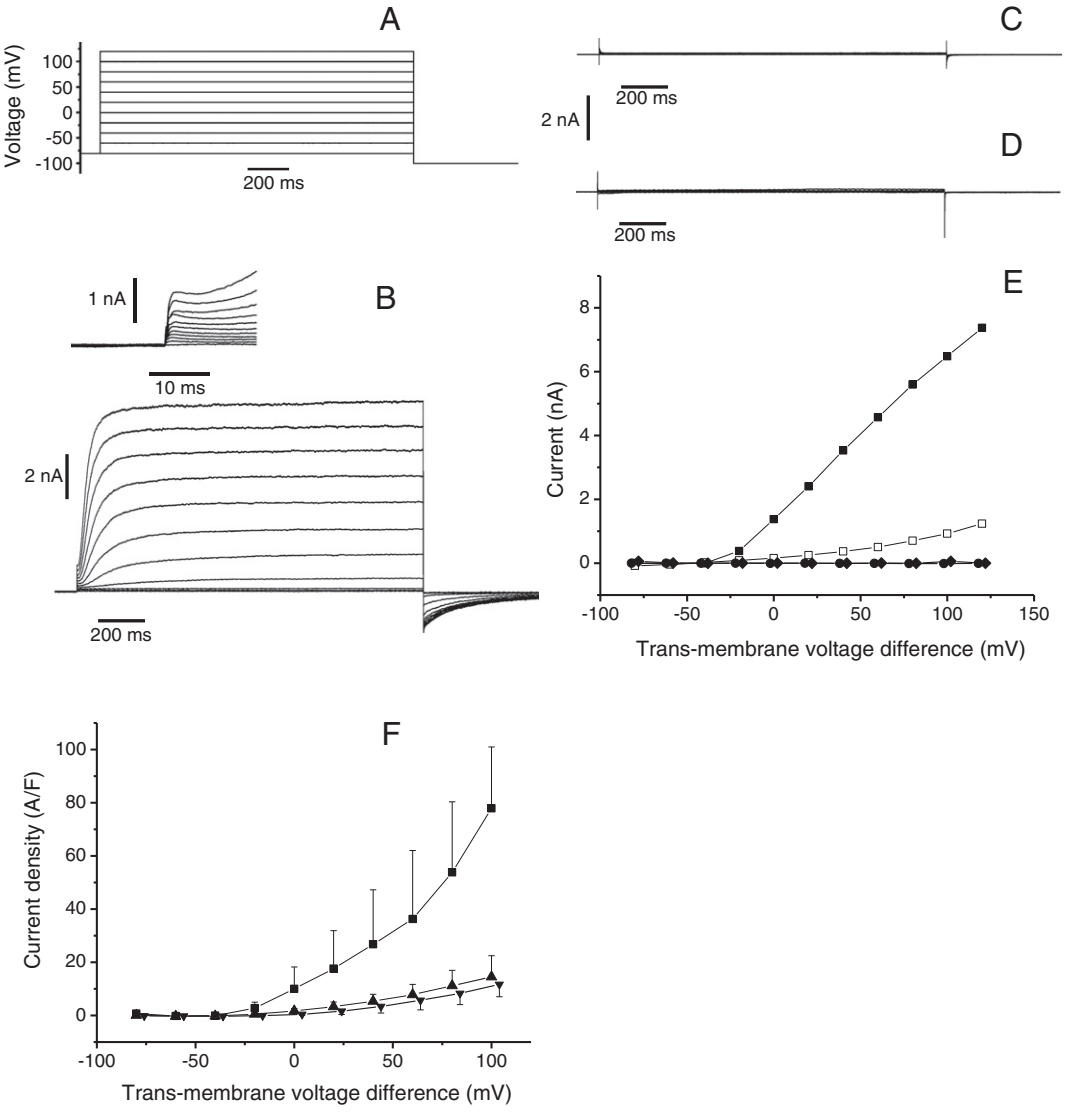

Fig. 1. Steady-state current voltage relations of BY-2 protoplasts in the physiological voltage range. Protoplasts clamped in the whole cell configuration were challenged with a series of voltage pulses (shown in A for all media combinations except for experiments with Na^+ in the pipette medium) and whole cell currents elicited by this protocol were recorded (representative example with P1/B1 media (250/12.5 mM K^+) shown in B; inset shows detail of main figure at an enlarged scale). Time-dependent outward currents were absent when media contained TEA^+ and TBA^+ instead of K^+ (C and D, respectively). Current voltage relations derived from recordings B–D are presented in E (squares: media P1/B1 (250/12.5 mM K^+); circles: P2/B2 (250/12.5 mM TEA^+); diamonds; P3/B3 (250/12.5 mM TBA^+); solid squares represent steady-state currents after leak subtraction, open squares currents after 10 ms pulse length (including the leak). In F, average current density is plotted against voltage for experiments with 250 mM K^+ (squares; P1), Rb^+ (upwardly-directed triangles; P4) and Na^+ (downwardly directed triangles; P5) in the pipette solution and 12.5 mM K^+ in the bath (B1). Error bars denote SEM values (3 replicates each). With Na^+ in the pipette, the same voltage protocol as shown in A was used, but with an offset of +4 mV due to *ex-post* correction of liquid junction potential.

potential', E_I) was considered to be the reversal potential associated with field-induced pores (a detailed account for the justification of this approach is given in the Discussion). When the prepulse was hyperpolarizing (−150 mV and −600 mV, respectively) the ramp started at that voltage with a positive slope (40 mV/ms change in command voltage; final voltage +150 mV and +600 mV, respectively). In Fig. 3A–C typical examples of plots obtained with different monovalent cations (K^+, TEA^+ and TBA^+) are depicted as obtained under these conditions. In these individual experiments, intersection potentials were determined to be −22, −10 and −13 mV, respectively. Similar results were obtained when depolarizing prepulses (+150 mV and +600 mV) were applied, followed by a voltage ramp with a negative slope (−40 mV/ms; final voltage −150 mV and −600 mV, respectively), indicating that pores induced by membrane de- and hyperpolarization had very similar properties. A synopsis of the intersection potential data including statistics is given in Table 2. Since the same cation gradient was imposed in all experiments and concentrations of all other ions remained constant, the absolute value of the reversal potential is a direct indicator for the selectivity to monovalent cations. Intersection potential was most negative with K^+, indicating that permeability to K^+ was higher than to the large organic cations. Note also that all values were in the negative voltage range, i.e. closer to the Nernst potential of the cation than to that of the counter-ion, Cl^-. Obviously, even large organic cations such as TEA^+ and TBA^+ were transported more readily than a small, highly mobile anion like chloride! Additionally, data for the LJP (with a negative sign, since the LJP is defined as bath with respect to pipette medium, opposite in polarity to the definition of command voltage in patch-clamp experiments) are given; these values correspond to the equilibrium voltage that would evolve at the interface of bath and pipette medium (i.e. at this voltage electrodiffusion of all ions is equally fast and, hence, ionic currents cancel each other out). Note

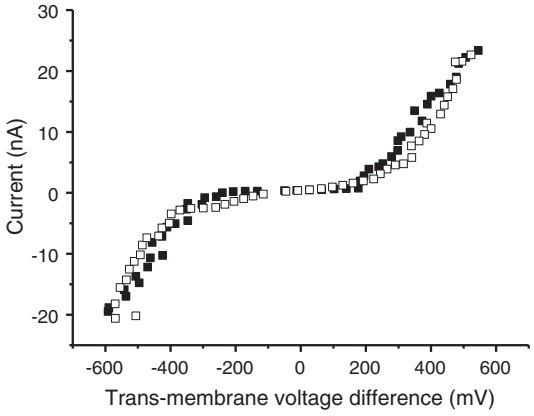

Fig. 2. Current voltage relations elicited by a series of 10 ms voltage pulses. Currents recorded at the end of the pulses are plotted as a function of the trans-membrane voltage drop (after correction for the voltage divider effect; see text, 2.1), with 250/12.5 mM K^+ (P1/B1, closed squares) and 250/12.5 mM TEA^+ (P2/B2, open squares).

again that setting the potential difference between pipette and bath to zero once the pipette tip was lowered into the bath also eliminated the LJP, but an offset was adjusted between the electrodes in order to correct for this effect (see 2.2)). Any deviation of the intersection potential from (−LJP) is due to the local microenvironment (or, rather, 'nanoenvironment'), i.e. most likely due to the properties of field-induced pores (e.g. size of the pores, properties of inner walls; membrane surface at the vicinity of the pore etc.).

In a separate set of experiments, permeability of field-induced pores to various alkali cations was tested under bi-ionic conditions. To this end, K^+ in the pipette – but not in the bath – was replaced by either Rb^+, Na^+ or Li^+. Representative examples for current–voltage relations obtained under these conditions are shown in Fig. 3D–F. When intracellular K^+ was substituted with Na^+ or Rb^+, the intersection potential remained unchanged within limits of accuracy, indicating that pores were equally permeable to K^+, Na^+ and Rb^+ (Table 2). However, with Li^+ in the pipette a significant negative shift of the intersection potential with respect to the other experiments was observed. This ion was apparently passing more readily through the pores than all the other monovalent cations tested in this study.

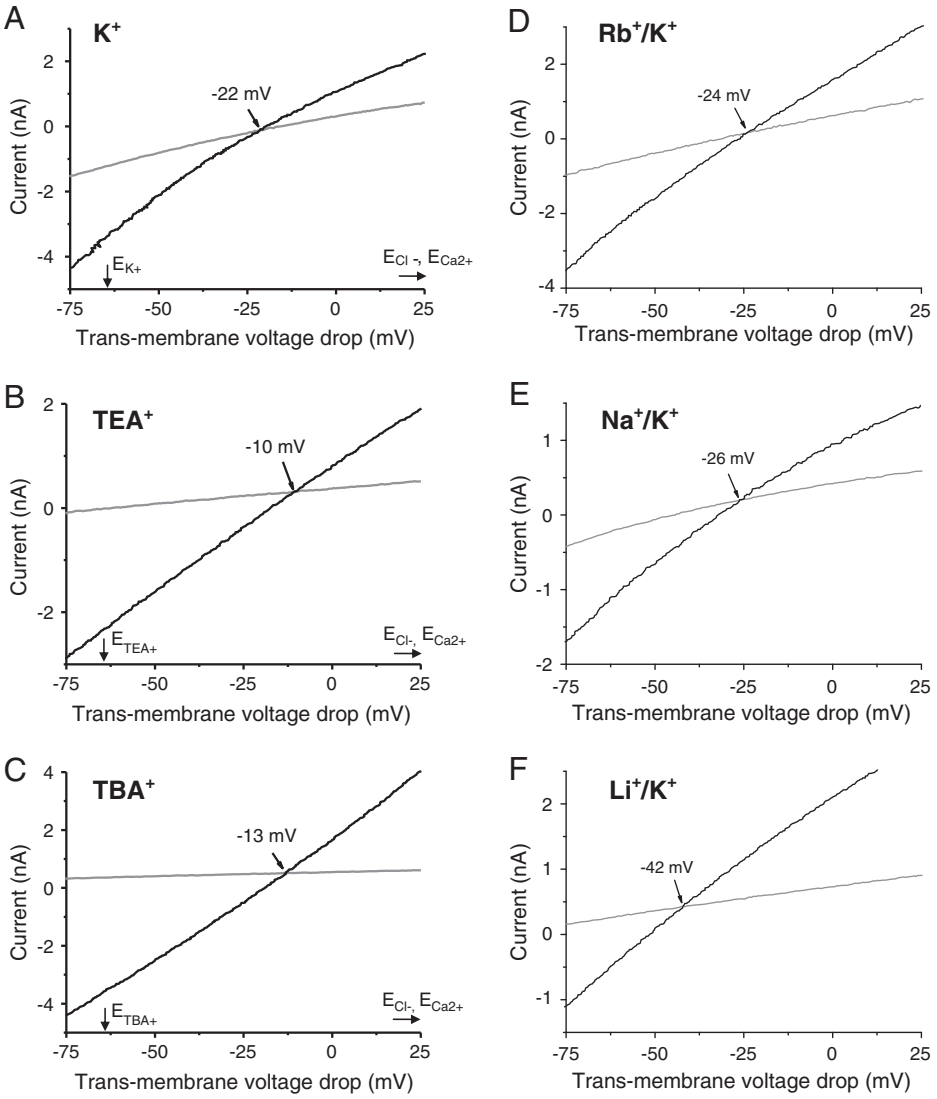

Fig. 3. Superposition of current–voltage relations obtained by ramp protocols following a 10 ms prepulse to −150 mV (grey traces) and −600 mV command voltage (black traces), respectively. For each of the various combinations of solutions (compare Table 1) a representative example was selected (only a limited voltage range required to identify E_I is shown). P1/B1 (A); P2/B2 (B); P3/B3 (C); P4/B1 (D); P5/B1 (E); P6/B1 (F). Only monovalent cations present in pipette/bath solution at concentrations of 250/12.5 mM are given on top of each figure. Intersection potentials marked by arrows are indicated in each of the figures. Nernst potentials E_{K+}, E_{TEA+} and E_{TBA+} in A, B, and C, respectively, were −65 mV. E_{Cl-} was +47 mV and E_{Ca2+} was +131 mV in A-F. For more details, see text.

3.4. Selectivity of field-induced pores to Ca^{2+}

The experiments reported above were performed in the presence of a steep, inwardly-directed Ca^{2+} gradient. Calcium was buffered to sub-micromolar values in the pipette medium in order to mimick physiological conditions; however, in the bath a rather high Ca^{2+} level (5 mM) was maintained to facilitate seal formation and preserve seals during pulse application [8]. For a quantitative interpretation of intersection potentials obtained with the various monovalent cations it was mandatory to infer the Ca^{2+} permeability of the cellular membrane in the electroporated state and, in turn, the contribution of Ca^{2+} fluxes to intersection potentials. To this end, monovalent cations in pipette and bath solutions were replaced by Ca^{2+}, so that a very high Ca^{2+} concentration was adjusted inside the cell. From a technical viewpoint it was difficult to establish and maintain the whole cell configuration of the patch clamp technique under these conditions since the membrane at the pipette tip tended to reseal immediately. However, by using large pipette tips (tip resistance <1MOhm) and applying slight overpressure in the pipette during the experiment, electrical access to the cell interior could be maintained for several minutes, at least in part of the protoplasts. Interestingly, the current response elicited by 10-ms-pulses in these cells was very similar to that measured in the presence of monovalent cations (Fig. 4), despite the rather unphysiologically high Ca^{2+} concentration. A 10-ms-pulse to −150 mV elicited a transient capacitive inward current that decayed within 1–2 ms (Fig. 4A), whereas a pulse to −600 mV command voltage induced pore formation and, in turn, inward current increasing with time that was superimposed on the capacitive current spike (compare e.g. [8]). Note that the effective voltage drop (Fig. 4B, top panel, continuous trace) deviated considerably from the command voltage (dotted line) due to a voltage drop at the access resistance [8].

This result indicates that Ca^{2+} does not protect the membrane against field-induced structural changes that lead to membrane permeabilization (or the protective effect is just a minor one).

Fig. 5 shows the result of a successful voltage ramp experiment performed in the same way as described above (hyperpolarizing prepulses followed by positive-going ramps). Note that the reversal potential was again in the negative voltage range, indicating that Ca^{2+} passed the membrane more readily than chloride. This is in line with the results presented above. On average, the reversal potential was about −6 mV independent of the polarity of the ramp (see also Table 2; media P7/B4).

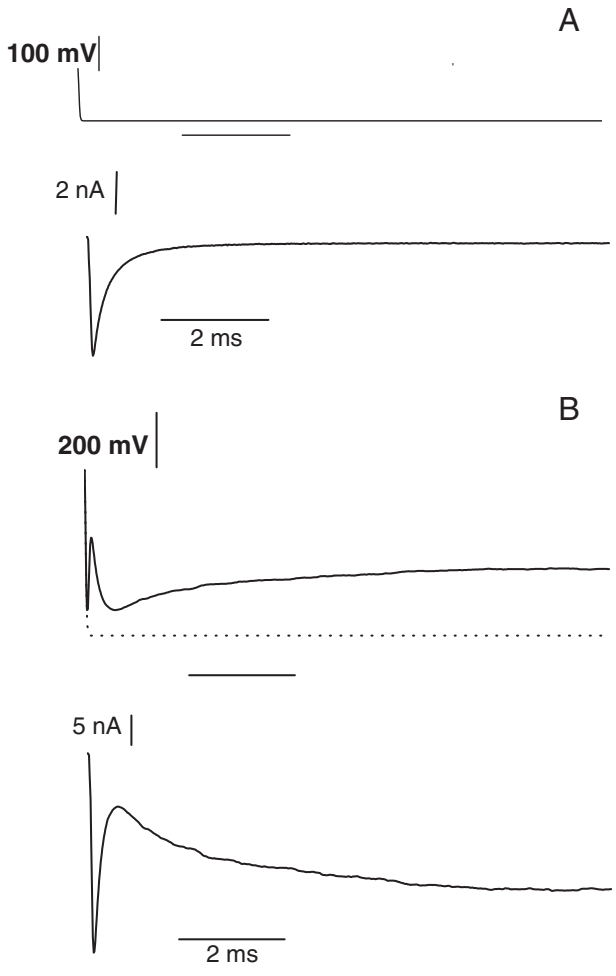

Fig. 4. Voltage pulses and current response of a BY-2 protoplast with monovalent cations in pipette and bath solution replaced by Ca^{2+} (media P7/B4). The voltage was stepped to −150 mV and −600 mV from a holding potential of 0 mV as shown in upper panels in A and B, respectively. In B, both the command voltage (dotted line) and the actual trans-membrane voltage drop (continuous line) are depicted. Lower panels show the respective current response of the protoplast. For more details, see text.

3.5. Quantitative evaluation of intersection potentials

Intersection potentials presented in the preceding paragraphs allow calculation of relative permeabilities of the electroporated membrane according to the Goldman-Hodgkin-Katz equation using the extended version of Piek [11] that takes both mono- and divalent cations into account. When the Cl^- permeability is set to 1, a value for the relative Ca^{2+} permeability can be calculated from the intersection potential in $CaCl_2$ media free of monovalent cations (ignoring permeability to all other ions, including Mg^{2+}). Subsequently, permeabilities for K^+, TEA^+ and TBA^+ were accessible from intersection potentials recorded in the presence of these ions at a fixed Ca^{2+} and Cl^- permeability retrieved from the above calculation. Finally, remaining permeabilities for the other alkali cations (Na^+, Rb^+, Li^+) are assessed from intersection potentials obtained at bi-ionic conditions with these ions in the pipette medium. The result is summarized in Table 2. Surprisingly, the highest permeability was found for Ca^{2+}, followed by Li^+, K^+, Na^+ and Rb^+ and finally TEA^+ and TBA^+. The resulting selectivity sequence is as follows:

$$Ca^{2+} > Li^+ > Rb^+ \approx K^+ \approx Na^+ > TEA^+ \approx TBA^+ > Cl^-$$

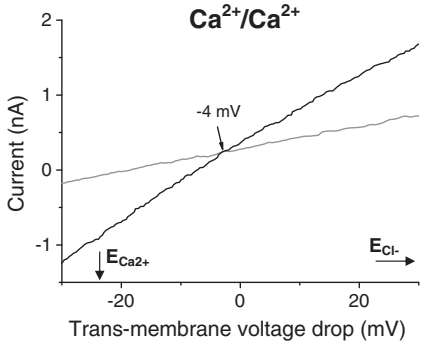

Fig. 5. Determination of the intersection potential with Ca^{2+} being the dominating cation in pipette and bath solution (media P7/B4). The representative experiment is evaluated and presented in the same way as described for other combinations of solutions in the legend to Fig. 3. Nernst potential of Ca^{2+} (E_{Ca2+}): −24 mV; E_{Cl^-}: +61 mV.

4. Discussion

4.1. Is the intersection potential the most adequate parameter to assess the ion selectivity of electric field-induced pores?

Calculation of (relative) ion permeabilites from intersection potentials is based on the assumption that the background conductance of the membrane, plus the leak conductance at the membrane-glass interface, remain unaltered by the field pulse, and that the conductance of field-induced pores is simply additive. Most likely processes occurring at the membrane during exposure to supra-physiological voltages are oversimplified by this approach. In fact, in a previous publication [8] it was demonstrated that K^+ channel activity in BY-2 cells is reduced when extreme voltages are applied, most likely due to the influx of Ca^{2+}. Alternatively, the reversal potential of the IV curve recorded in the electroporated state, that was usually more negative than the intersection potential, could be taken as the voltage at which no net currents pass through open, field-induced pores. This would be the correct value if the background membrane conductance was completely blocked by the electric field, which appears to be an even unlikely boundary condition. The 'true value' is most likely somewhere in between. However, there are several indications for the intersection potential being the most adequate choice for the reversal potential of currents passing through field-induced pores that could be made. Most importantly, in cases where the contribution of background currents was very low and, hence, the reversal potential of the electroporated membrane IV curve was identical to the intersection potential, this value was close to intersection potentials measured on other protoplasts (data not shown). Moreover, there is always a background conductance associated with the imperfect seal that tends to increase, rather than decrease, when extreme voltages are applied.

Therefore, it seems most adequate to make use of the intersection potentials as the best parameter to approximate the reversal potential of open-pore current voltage relations.

4.2. Practical implications of the results

Field-induced poration of the cellular membrane initiates ion fluxes into and out of the cell and, in turn, a massive change in the ionic milieu of the cytosol. This effect is of practical relevance in biotechnology and medicine and, hence, has been a subject of both experimental and theoretical work. In previous studies on this issue (including a very recent one by Movahead and Li [19]) it has always been assumed that membrane pores are large aqueous 'holes' with little ion selectivity, i.e. pore formation would be associated with an (at least partial) breakdown of both cation and anion concentration gradients, especially with a pulse length of several ms. The present study has demonstrated that this basic assumption is not correct, at least not for BY-2 cells. Rather, the membrane in the electroporated state is quite cation selective. Therefore, administration of pulsed electric fields by two external electrodes which is the 'usual' procedure in biotechnology [20] will predominantly induce cation fluxes across the membrane (K^+ and Ca^{2+} influx at the negatively charged pole of a spherical cell and K^+ efflux at the positive pole, respectively). Ca^{2+} influx under these conditions has been demonstrated experimentally in BY-2 cells [21]. Due to the poor anion permeability of the pores, anions will contribute little to ion fluxes. Work of Pakhomov and Pakhomova on GH3 cells [5] and Dyachok et al. on pig ventricular myocytes [22] suggest that this conclusion also applies to mammalian cells, with Na^+ influx (Na^+ being equally permeable as K^+, at least in BY-2 cells) as an additional component to be taken into account.

How can one make use of these findings? The data suggest that electroporation is especially useful to introduce divalent cations into cells. This has been demonstrated experimentally for Ca^{2+} influx during and after the application of microsecond pulses [21]. There is a recent report in the literature showing that PEFs can be employed to introduce Mg^{2+} into yeast cells [23]. Further applications of this kind should be considered (see also [20]).

While changing the ionic milieu of the cytosol may be desirable under some conditions, other applications (especially reversible electroporation e.g. for cell transfection) require protection of the ionic composition of the cytosol. Ionic fluxes during and after the pulse are likely to be reduced with low Ca^{2+} and Na^+ concentrations in the bath during pulse application. Further work on this issue is required, including a more detailed analysis of the average life time of the pores once the membrane potentials return to moderate values.

Since membrane permeation tends to be hampered by negative charge, the data seem to suggest that electroporation is less suitable to introduce anions into cells, and least suitable for the transport of negatively charged macromolecules. Strikingly, though, the technique has most frequently and successfully been used to transport DNA, a poly-anion, into cells. This apparent contradiction can only be resolved by assuming that DNA is not transported through the 'ordinary' membrane pores that leave their signature in patch clamp experiments, but rather by a very different mechanism, e.g. as suggested in a recent publication [24]. It has to be kept in mind that the data presented here are overall values that only reflect the properties of the majority of the pores. In fact, pores (or other transport pathways) may exist that contribute little to overall conductance and have properties completely different from those reported here.

4.3. Implications of the results for molecular properties of field-induced pores

Most importantly, this study provides an empirical dataset characterizing the electroporated cellular membrane during the application of a PEF. Selectivity data allow conclusions on the properties of these pores, as previously demonstrated for ion channels [22,25–27], porins [28,29], and nanoporous materials [30,31], e.g. silicon membranes. The most simple and straightforward approach to interprete reversal potentials in terms of ion transport through pores is provided by the Nernst-Planck formalism, assuming electroneutrality throughout the lumen of the pore and ignoring interactions of ions with each other and the wall of the pores. However, reversal potentials for the various combinations of solutions tested here deviated considerably from (−) liquid junction potentials (Table 2) that would be expected for a pure electrodiffusion process. An alternative is provided by the Goldman–Hodgkin–Katz equation that combines the Nernst-Planck formalism with the Poisson equation (for a more detailed discussion see [28,29]) and is based on the assumption of a linear drop of the trans-membrane potential difference across the pore, as well as independent movement of monovalent ion species (and additionally Ca^{2+} [11]). Relative ion permeabilities (Table 3) were calculated here based on this formalism. A qualitative comparison of the data suggests that

Table 3
Relative permeabilities (P_x/P_{Cl^-}; mean values) of major ions tested in this study calculated according to Eq. (4).[a]

Ion species X	P_x/P_{Cl^-}	
	Negative-going prepulse, ramp +40 mV/ms (c.v.)	Positive-going prepulse, ramp -40 mV/ms (c.v.)
K^+	3.4	2.8
Rb^+	3.8	n.d.
Na^+	3.4	n.d.
Li^+	6.3	n.d.
TEA^+	1.7	1.4
TBA^+	1.9	1.7
Ca^{2+}	6.4	6.4
Cl^-	1	1

[a] c.v. = command voltage.

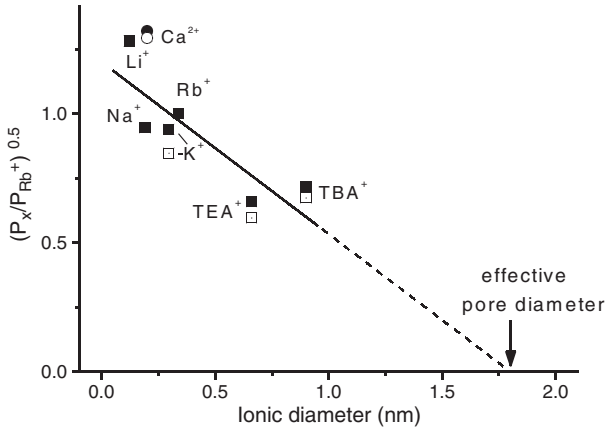

Fig. 6. Plot of the square root of the membrane permeability normalized to Rb^+ permeability against the ionic diameter for the various cations tested in this study. Hyperpolarization- and depolarization-induced pores are indicated by solid and open symbols, respectively. Solid line represents best fit of the data with Eq. (5) (correlation coefficient $R^2 = 0.6$). Intersection with x-axis indicates the size of the effective diameter of the pore (about 1.8 nm). The values for Ca^{2+} are also plotted for comparison, but were not included in the fit.

besides preferring cations to anions the pores were clearly selecting for size, since small alkali cations were more permeable than the large organic ones. Moreover, it is interesting to note that Li^+ permeability of the membrane was roughly two times that of K^+. The ionic diameter of Li^+ is much smaller than that of K^+ (0.12 nm versus 0.27 nm). This is in accordance with permeability being inversely related to size, but only if the hydration shell of the ions is stripped off upon entrance to the pore. By contrast, the hydrodynamic diameter of Li^+ is considerably larger than that of K^+ (0.48 versus 0.25 nm). Hence, if the ions were penetrating without losing their hydration shell, K^+ would be expected to be more permeable than Li^+, contrary to what was observed here. Consistently, the square root of the monovalent cation permeability P_x (normalized to the value measured with Rb^+) was inversely related to the ionic diameter (Fig. 6). Data in Fig. 6 could be fitted with a simple equation derived by Dwyer et al. [27] that is based on the 'excluded volume effect'; assuming cylindrical shape of the pore, permeability is proportional to the cross-sectional area that is not taken by the permeating ion ($P_x \sim (\delta_{pore} / 2 - \delta_x / 2)^2$), and in terms of relative permeability can be expressed as [27]:

$$\left(\frac{P_x}{P_{Rb+}}\right)^{0.5} = \frac{\delta_{Pore} - \delta_x}{\delta_{Pore} - \delta_{Rb+}} \quad (5)$$

with δ_{Pore} being the effective pore diameter and δ_x and δ_{Rb+} being the ionic diameters of the ion species x and Rb^+, respectively (determined from crystal dimensions according to the method of Pauling; cited after [25]). From this plot an effective pore diameter of ~1.8 nm was inferred. Previously, this formalism has successfully been applied to describe the permeability of cation selective pores [25–27]. Although the equation suggests selection purely by size (friction), negative charges must be present at the inward and outward membrane surface to select for cations *versus* anions, and to provide the energy for stripping off the hydration shell. Deviations of individual values from the straight line in Fig. 6 may be due to electrostatic effects; e.g., the relative permeability to Li^+ is higher than predicted from equation 5, possibly due to the high charge density of this ion.

Further experimental data are required to analyse pore properties in more detail as e.g. done previously for the porin OmpF [28,29].

The permeability data reported here for tobacco protoplasts exposed to 10 ms PEFs agree remarkable well with those reported by Pakhomov and Pakhomova for GH3 cells following treatment with a nanosecond pulse [5], except for Li^+ that was more permeable than K^+ in BY-2 protoplasts, whereas in GH3 cells it was exactly opposite. The general good agreement of results presented here for ms pulsed electric fields with previous work done with much shorter pulse length is clearly at variance with the assumption frequently found in the literature (and supported by current theories on the molecular mechanism of pore formation) that pore properties change fundamentally with pulse length from ns to ms scale [32,33]. Rather, it appears now that at least the majority of field-induced pores have fairly uniform properties independent of cell type and field exposure time. Cation selectivity of lipid-lined pores may result from polar phospholipid headgroups carrying negative charges, as discussed in more detail previously [8], but alternative interpretations are also feasible. In fact, field induced pores seem to share many properties with non-selective cation channels, and the question arises whether there is a mechanistic and structural link between these phenomena (A. Pakhomov, personal communication). 'Irregular' activity of cation-selective channels may be elicited at extreme voltages. During hyperpolarization, massive Ca^{2+} influx may additionally trigger Ca^{2+-} activated channels (see also Beilby, [34]). NtORK, the cation channel that dominates membrane conductance in the physiological voltage range, is an unlikely candidate, though, since this channel is inhibited by both elevated cytosolic Ca^{2+} concentrations and by pulsed electric fields (which may have a common origin since Ca^{2+} influx into the cytosol through electric field-induced pores tends to inactivate K^+ channels, at least temporarily; [8]). Moreover, the massive increase in membrane conductance reported here and in previous publications occurs both with hyper- and with depolarization of the membrane once threshold potentials are exceeded. Current–voltage curves are nearly symmetrical around zero voltage, but Ca^{2+} influx (and, in turn, activation of ion channels by an increase in cytosolic Ca^{2+}) would be favoured by membrane hyperpolarization, and much less so by depolarization. Still, the role of ion channels for electroporation will be an issue of further research.

Acknowledgements

This work was supported by the Karlsruhe Institute of Technology in the framework of the German Excellence Initiative (SRG 60–1), and by the German Ministry of Science and Education (BMBF grant no. 0315664B) to LHW. Thanks are due to Mrs Sarah Rocke for excellent technical assistance and to Mr. Sebastian Schindler and Mrs. Sina Schönwälder for their assistance at different stages of this project. I would also like to thank Prof. Andrei Pakhomov and Mrs Betsy W. Gregory from Frank C. Reidy Research Center for Bioelectrics, Norfolk, Va., USA for critical reading of the manuscript.

References

[1] E. Neumann, K. Rosenheck, Permeability changes induced by electric impulses in vesicular membranes, J. Membr. Biol. 10 (1972) 279–290.
[2] U. Zimmermann, G. Pilwat, F. Riemann, Dielectric breakdown of cell membranes, Biophys. J. 14 (1974) 881–889.
[3] D.P. Tieleman, The molecular basis of electroporation, BMC Biochem. 19 (2004) 5–10.
[4] M. Tarek, Membrane electroporation: a molecular dynamics simulation, Biophys. J. 88 (2005) 4045–4053.
[5] A.G. Pakhomov, O.N. Pakhomova, Nanopores, a distinct transmembrane passageway in electroporated cells, in: A.G. Pakhomov, D. Miclavcic, M.S. Markov (Eds.), Advanced Electroporation Techniques in Biology and Medicine, CRC Press, Boca Raton etc, 2010, pp. 177–194.
[6] A.G. Pakhomov, A. Bowman, B. Ibey, F. Andre, O. Pakhomova, K. Schoenbach, Lipid nanopores can form a stable, ion channel-like conduction pathway in cell membrane, Biochem. Biophys. Res. Com. 385 (2009) 181–186.
[7] O.M. Nesin, O.N. Pakhomova, S. Xiao, A.G. Pakhomov, Manipulation of cell volume and membrane pore comparison following single cell permeabilization with 60- and 600-ns electric pulses, Biochim. Biophys. Act. Biomem. 1808 (2011) 792–801.
[8] L.H. Wegner, B. Flickinger, C. Eing, T. Berghöfer, P. Hohenberger, W. Frey, P. Nick, A patch clamp study on the electro-permeabilization of higher plant cells: Supra-physiological voltages induce a high-conductance, K^+ selective state of the plasma membrane, Biochim. Biophys. Act. Biomem., 1808, 2011, pp. 1728–1736.
[9] L.H. Wegner, W. Frey, S. Schönwälder, A critical evaluation of whole cell patch clamp studies on electroporation using the voltage sensitive dye ANNINE-6, Bioelectrochem 92 (2013) 42–46.

[10] L.H. Wegner, S. Schönwälder, Electroporation of plant cells studied with the patch clamp technique, Proceedings of EAPPC/BEAMS2012, 30 Sept.-04 Oct. 2012, Karlsruhe, Germany, 2012, online available at http://www.eappc-beams2012.org/EAPPC-BEAMS2012-Conference-Proceedings.zip (retrieved 08/03/2013).
[11] T. Piek, Ionic and electrical properties, in: T. Piek (Ed.), Insect Muscle, Academic Press, London, 1975, pp. 281–336.
[12] K.J. Führ, W. Warchol, M. Gratzl, Calculation and control of free divalent cations in solutions used for membrane fusion studies, Methods Enzymol. 221 (1993) 149–157.
[13] R.A. Robinson, R.H. Stokes, Electrolyte Solutions, second ed. Dover Pubn. Inc., 2002
[14] E. Neher, Correction for liquid junction potentials in patch clamp experiments, Methods Enzymol. 207 (1992) 123–130.
[15] T. Sano, D. Becker, N. Ivashikina, L.H. Wegner, U. Zimmermann, M.R.G. Roelfsema, R. Nagata, R. Hedrich, Plant cells must pass a K^+ threshold to re-enter cell cycle, Plant J. 50 (2007) 401–413.
[16] B. Van Duijn, D.L. Ypey, K.R. Libbenga, Whole-cell K^+ currents across the plasma membrane of tobacco protoplasts from cell-suspension cultures, Plant Physiol. 101 (1993) 81–88.
[17] H. Stoeckel, K. Takeda, Plasmalemma voltage-activited K^+ currents in protoplasts from tobacco BY-2 cells: possible regulation by actin microfilaments? Protoplasma 220 (2002) 79–87.
[18] L.H. Wegner, A.H. De Boer, Activation kinetics of the K^+ outward rectifying conductance (KORC) in xylem parenchyma cells from barley roots, J. Membr. Biol. 170 (1999) 103–119.
[19] S. Movahead, D. Li, Electrokinetic transport through the nanopores in cell membrane during electroporation, J. Coll. Interf. Sci. 369 (2012) 442–452.
[20] G. Saulis, Electroporation of cell membranes: the fundamental effects of pulsed electric fields in food processing, Food Eng. Rev. 2 (2010) 52–73.
[21] V.L. Soukhorukov, J.M. Endter, D. Zimmermann, R. Shirakashi, S. Fehrmann, M. Kiesel, R. Reuss, D. Becker, R. Hedrich, E. Bamberg, T. Roitsch, U. Zimmermann, Mechanisms of electrically mediated cytosolic Ca^{2+} transients in aequorin-transformed tobacco cells, Biophys. J. 93 (2007) 3324–3337.
[22] O. Dyachok, P. Zhabyeyev, T.F. McDonald, Electroporation-induced inward current in voltage-clamped pig ventricular myocytes, J. Membr. Biol. 238 (2010) 69–80.
[23] U. Pankiewicz, J. Jamroz, Effect of pulsed electric fields upon accumulation of magnesium in *Saccharomyces cerevisiae*, Eur. Food Res. Technol. 231 (2010) 663–668.
[24] M. Yu, W. Tan, H. Lin, A stochastic model for DNA translocation through an electropore, Biochim. Biophys. Act 1818 (2012) 2494–2501.
[25] D.-M. Liu, D.J. Adams, Ionic selectivity of native ATP-activated (P2X) receptor channels in dissociated neurons from rat parasympathetic ganglia, J. Physiol. 534 (2) (2001) 423–435.
[26] N. Burnashev, A. Villarroel, B. Sakmann, Dimensions and ion selectivity of recombinant AMPA and kainite receptor channels and their dependence on Q/R site residues, J. Physiol. 496 (1) (1996) 165–173.
[27] T.M. Dwyer, D.J. Adams, B. Hille, The permeability of the endplate channel to organic cations in frog muscle, J. Gen. Physiol. 75 (1980) 469–492.
[28] A. Alcaraz, E.M. Nestorovich, M. Aguilella-Arzo, V.M. Aguilella, S.M. Bezrukov, Salting out the ionic selectivity of a wide channel: the asymmetry of OmpF, Biophys. J. 87 (2004) 943–957.
[29] A. Alcaraz, E.M. Nestorovich, M.L. Lopez, E. Garcia-Gimenez, S.M. Bezrukov, V.M. Aguilella, Diffusion, exclusion, and specific binding in a large channel: a study of OmpF selection inversion, Biophys. J. 96 (2009) 56–66.
[30] J. Cervera, A. Alcaraz, B. Schiedt, R. Neumann, P. Ramirez, Asymmetric selectivity of synthetic conical nanopres probed by reversal potential measurments, J. Phys. Chem. 111 (2007) 12265–12273.
[31] R. Ishimatsu, J. Kim, P. Jing, C.C. Striemer, D.Z. Fang, P.M. Fauchet, J.L. McGrath, S. Amemiya, Ion-selective permeability of an ultrathin nanoporous silicon membrane as probed by scanning electrochemical microscopy using micropipette-supported ITIES tips, Anal. Chem. 82 (2010) 7127–7134.
[32] Q. Hu, R.P. Joshi, K.H. Schoenbach, Simulations of nanopore formation and phosphatidylserine externalization in lipid membranes subjected to a high-intensity, ultrashort electric pulse, Phys. Rev. E 72 (2005) 10–15.
[33] W. Krassowska, P.D. Filev, Modeling electroporation in a single cell, Biophys. J. 92 (2007) 404–417.
[34] M.J. Beilby, Modeling oscillations of membrane potential difference, in: S. Mancuso, S. Shabala (Eds.), Rhythms in Plants: Phenomenology, Mechanisms, and Adaptive Significance, Springer, Berlin, Heidelberg, 2007, pp. 341–355.